INTERNATIONAL JOURNAL FOR NUMERICAL METHODS IN FLUIDS
Int. J. Numer. Meth. Fluids 2006; **51**:1041–1057
Published online 24 March 2006 in Wiley InterScience (www.interscience.wiley.com). DOI: 10.1002/fld.1197

Analysis of fluid flow through micro-fluidic devices using characteristic-based-split procedure

Bayram Celik[‡] and Firat Oguz Edis[*,†]

Faculty of Aeronautics and Astronautics, Istanbul Technical University, Maslak, Istanbul 34469, Turkey

SUMMARY

Gas flow in micro-electro-mechanical systems can be considered as rarefied since the ratio of free molecular path length to the characteristic length of the device is high. It is possible to analyse these flows using a conventional Navier–Stokes solver with modified boundary conditions to account for temperature-jump and slip-velocity on solid walls. In this study, characteristic-based-split (CBS) algorithm is modified to account for slip-velocity and temperature-jump boundary conditions in order to perform compressible flow analysis for a micro sized geometry. The CBS algorithm is a split procedure which yields a unified solution method valid for both compressible and incompressible flows. To verify the modified CBS solver, straight micro channel and micro step duct geometries are selected as test cases. To reduce the size of the implicit part of the algorithm, pseudo-quadratic velocity/linear pressure elements (pP2P1) are employed. The results obtained using CBS algorithm, are compared with other analytical and computational results available in the literature. It is shown that this implementation of the CBS algorithm is applicable and effective for micro gas flows. It is also shown that, increasing Knudsen number results in increased temperature-jump and slip-velocity. This effect, however, is limited, especially for high Mach number flows. Copyright © 2006 John Wiley & Sons, Ltd.

KEY WORDS: rarefied flow; temperature-jump; slip-velocity; compressible flow; microflow; characteristic-based-split (CBS) algorithm

1. INTRODUCTION

Micro-electro-mechanical systems (MEMS) are combinations of electrical and mechanical devices which have characteristic lengths in the range of 1 mm–1 μm [1]. During the fluid flow in these tiny machines, friction, electrostatic forces and viscous effects become more dominant than inertial forces [1]. Knudsen number (Kn), the ratio of the molecular mean free

*Correspondence to: Firat Oguz Edis, Faculty of Aeronautics and Astronautics, Istanbul Technical University, Maslak, Istanbul 34469, Turkey.
†E-mail: edis@itu.edu.tr
‡E-mail: celikbay@itu.edu.tr

Contract/grant sponsor: Istanbul Technical University; contract/grant number: 1839

Received 2 June 2005
Revised 24 November 2005
Accepted 18 January 2006

path length to the characteristic length, is the key parameter for the flow over these type of devices. As the value of *Kn* increases, the difference between the results predicted by the continuum model and the actual flow increases due to the increasing effects of boundary slip, thermal creep, rarefaction, viscous dissipation, compressibility, intermolecular forces and other unconventional effects [1–4].

If *Kn* is smaller than 10^{-3}, the regime is called continuum regime and the flow can be simulated using conventional Navier–Stokes equations (N–S) solvers. If *Kn* is in the range of 10^{-3}–10^{-1}, the fluid flow is assumed to be in the slip regime and the flow can be still simulated using a N–S solver by modifying standard temperature-wall and no-slip boundary conditions [1]. Direct Simulation Monte Carlo Method (DSMC) is a good choice for analysis of high *Kn* flow problems. But, if *Kn* is smaller than 0.1, to use DSMC as a solver is relatively expensive compared to N–S solvers [2, 5].

In the present paper, compressible, internal flow through a straight micro channel and micro backward facing step geometry are simulated using characteristic-based-split (CBS) algorithm. To do this, the second-order slip-velocity of Beskok [4] and temperature-jump condition are employed on the wall within the CBS algorithm. To verify the solver, a straight micro channel flow is simulated. Then, the analyses for the micro backward facing step geometry are performed in order to understand rarefaction effects in the flow fields containing sharp gradients.

2. GOVERNING EQUATION

Compressible Navier–Stokes equations in conservation form in Cartesian co-ordinate systems (x_1, x_2) can be written as follows:

$$\frac{\partial \mathbf{V}}{\partial t} + \frac{\partial \mathbf{F}_i}{\partial x_i} + \frac{\partial \mathbf{G}_i}{\partial x_i} + \mathbf{Q} = 0, \quad i = 1, 2 \tag{1}$$

General form of the Navier–Stokes equation given above includes continuity, momentum and energy equations. In the equation given above $\mathbf{V}$, $\mathbf{F}_i$, $\mathbf{G}_i$ and $\mathbf{Q}$ denote dependent variable, convective flux (in x_i direction), diffusive flux and source term vectors, respectively. These vectors are in the following form:

$$\mathbf{V} = \begin{bmatrix} \rho \\ \rho u_1 \\ \rho u_2 \\ \rho e \end{bmatrix}, \quad \mathbf{F}_i = \begin{bmatrix} \rho u_i \\ \rho u_1 u_i + \delta_{1i} p \\ \rho u_2 u_i + \delta_{2i} p \\ u_i(\rho e + p) \end{bmatrix}, \quad \mathbf{G}_i = \begin{bmatrix} 0 \\ -\tau_{1i} \\ -\tau_{2i} \\ -(k\, \partial T/\partial x_i) - \tau_{ij} u_j \end{bmatrix}, \quad \mathbf{Q} = \begin{bmatrix} 0 \\ -\rho g_1 \\ -\rho g_2 \\ -\rho(g_i u_i + r) \end{bmatrix} \tag{2}$$

where ρ is the density, u_i is the velocity component in x_i direction, p is the pressure, T is the temperature, g_i is the ith component of the gravity acceleration, r is a heat source, k is the thermal conductivity, μ is the viscosity and δ_{ij} is the Kronecker delta function. The equations are completed by the gas state law given below

$$p = \rho R T \tag{3}$$

where R is the gas constant. τ_{ij} are related to velocity gradients linearly by the Stokes hypothesis as written below

$$\tau_{ij} = \mu \left[\left(\frac{\partial u_i}{\partial x_j} + \frac{\partial u_j}{\partial x_i} \right) - \delta_{ij} \frac{2}{3} \frac{\partial u_k}{\partial x_k} \right] \tag{4}$$

The total energy per unit mass is denoted with e (internal plus kinetic) and it is related to temperature and velocity through the following equation:

$$e = C_v T + u_i u_i / 2 \tag{5}$$

where C_v is the specific heat at constant volume.

3. SLIP-VELOCITY FORMULATION

The first-order approach of Maxwell's slip-velocity and Smoluchowski's temperature-jump boundary condition is given as follows [2]:

$$u_s - u_w = \frac{2 - \sigma_v}{\sigma_v} \frac{1}{\rho (2RT_w/\pi)^{1/2}} \tau_s + \frac{3}{4} \frac{Pr(\gamma - 1)}{\gamma \rho R T_w} (-q_t) \tag{6}$$

$$T_s - T_w = \frac{2 - \sigma_T}{\sigma_T} \left[\frac{2(\gamma - 1)}{\gamma + 1} \right] \frac{1}{R\rho (2RT_w/\pi)^{1/2}} (-q_n) \tag{7}$$

In the equations written above, subscripts s and w denote slip and wall (reference) values. q_n and q_t are the normal and tangential components of the heat flux. τ_s is the viscous stress component. Momentum and energy accommodation coefficients are denoted by σ_v and σ_T and Pr is the Prandtl number. In the present study, full diffuse reflection is assumed ($\sigma_v = \sigma_T = 1$). A second-order slip velocity boundary condition based on asymptotic analysis is proposed by Beskok and Karniadakis [3, 4]

$$u_s^* - u_w^* = \frac{2 - \sigma_v}{\sigma_v} \frac{Kn}{1 - bKn} \left(\frac{\partial u^*}{\partial n^*} \right)_w + \frac{3}{2\pi} \frac{(\gamma - 1)}{\gamma} \frac{Kn^2 Re}{Ec} \left(\frac{\partial T^*}{\partial s^*} \right)_w \tag{8}$$

In the equation above, b is the high-order slip coefficient and its value is determined analytically, Ec is the Eckert number and superscript $*$ denotes the variables in non-dimensional form. Local Knudsen number can be written in terms of local Mach (Ma) and Reynolds (Re) numbers as $Kn = \sqrt{(\pi\gamma/2)} Ma/Re$. Derivatives of the velocity and temperature in normal and tangential directions, respectively, are denoted with $\partial u/\partial n$ and $\partial T/\partial s$ in the equation.

4. CBS ALGORITHM

The split procedure has been used by many scientists for the solution of incompressible flow problems since its first introduction by Chorin [6] in finite difference formulation. An application of this split procedure to the compressible flow problems using finite element formulation was done by Zienkiewicz and Wu in 1992 [7]. Then, a general algorithm for both compressible and incompressible flow problems was introduced by Zienkiewicz and Codina in 1995 [8]. They have published several papers concerning the application of this new unified

algorithm and its modification in the following years [9, 10]. Finally the algorithm was named as 'CBS' [11].

The most important advantage of using CBS algorithm is that the incompressible and compressible N–S or Euler equations can be solved using the same code. There are many successful applications of the algorithm for solving the problems ranging from nearly incompressible, viscous flows through transonic to the flows with shock in high speed [12–15]. The results, obtained using the CBS algorithm, show that the algorithm behaves very well for different flow regimes (such as numerical simulation of incompressible flow, barotropic flow and compressible flow cases).

In this study, the CBS algorithm is used to analyse the compressible, rarefied internal flow through the micro geometries by modifying usual no-slip and temperature wall boundary conditions. Using standard Galerkin formulation for discretization of the governing equation in space causes numerical instabilities due to the convective term appearing in momentum equation. In CBS procedure, this effect is stabilized by discretizing the equations along the characteristic of the total derivative as explained with details in Reference [8]. Then three essential steps of the CBS algorithm are obtained by introducing a new auxiliary variable for the momentum equation [8]. Details of this procedure can be found in References [8, 9]. In the present study, semi implicit form of the CBS algorithm is used. The weak forms of the equations are given in Sections 4.1–4.4.

4.1. Fractional momentum equation

Multiplying the fractional momentum equation given in Reference [8] by an appropriate shape function W_u, integrating the viscous and the other terms coming from the discretization along the characteristics over the domain Ω yields

$$\int_\Omega W_u \Delta\tilde{U}_i \,\mathrm{d}\Omega = +\Delta t \left[-\int_\Omega W_u \frac{\partial}{\partial x_j}(u_j U_i)\,\mathrm{d}\Omega - \int_\Omega \frac{\partial W_u}{\partial x_j}\tau_{ij}\,\mathrm{d}\Omega - \int_\Omega W_u(\rho g_i)\,\mathrm{d}\Omega \right]^n + \frac{\Delta t^2}{2}\left[\int_\Omega \frac{\partial}{\partial x_l}(u_l W_u)\left(-\frac{\partial}{\partial x_j}(u_j U_i) + \rho g_i\right)\mathrm{d}\Omega\right]^n + \Delta t\left[\int_\Gamma W_u \tau_{ij} n_j \,\mathrm{d}\Gamma\right]^n \quad (9)$$

In the equation above, U_i^n is the ith component of the momentum at time n. n_j is the unit normal vector in x_j direction. Auxiliary momentum value in the direction of x_i is denoted with $\tilde{U}_i$ and $\Delta\tilde{U}_i = \tilde{U}_i - U_i^n$. The boundary term appearing in the equation above comes from integration by parts of the viscous term of the momentum equation.

4.2. Continuity equation

Choosing pressure shape function W_p as the test function and multiplying the continuity equation by it and integrating resulting equation over the domain Ω gives the following equation:

$$\begin{aligned}\int_\Omega W_p \Delta\rho \,\mathrm{d}\Omega &= -\Delta t \int_\Omega W_p \frac{\partial}{\partial x_i}\left(U_i^n + \theta_1 \Delta\tilde{U}_i - \theta_1 \Delta t \frac{\partial p^{n+\theta_2}}{\partial x_i}\right)\mathrm{d}\Omega \\ &= \Delta t \int_\Omega \frac{\partial W_p}{\partial x_i}\left[U_i^n + \theta_1\left(\Delta\tilde{U}_i - \Delta t \frac{\partial p^{n+\theta_2}}{\partial x_i}\right)\right]\mathrm{d}\Omega \\ &\quad -\Delta t\,\theta_1 \int_\Gamma W_p\left(U_i^n + \Delta\tilde{U}_i - \Delta t \frac{\partial p^{n+\theta_2}}{\partial x_i}\right) n_i \mathrm{d}\Gamma \end{aligned} \quad (10)$$

where $p^{n+\theta_2}$ is equal to $\theta_2 p^{n+1} + (1-\theta_2)p^n$. In the present study, weighting function θ_1 and θ_2 are selected to be 1. Pressure or density may be used as unknown in the continuity equation (10). In this study, pressure is used as unknown. Using the perfect gas law (3), the density variation term $\Delta\rho = \rho^{n+1} - \rho^n$ placed on the left-hand side of the continuity equation is replaced with pressure variation term

$$\Delta\rho = \frac{\Delta p}{RT_g} + \left(\frac{p^n}{RT_g} - \frac{p^n}{RT^n}\right) \tag{11}$$

It is required to guess a temperature value T_g instead of unknown value of T at time $n+1$ to uncouple the resulting continuity equation and the energy equation. It is reported in Reference [10], this approach works well if only steady state is of interest as in this study. Details of this approach are given in Section 4.5.

4.3. Final step of the momentum equation

Using the pressure values at time $n+1$ obtained from continuity equation (10) and auxiliary momentum value, the momentum values at time $n+1$ are obtained from the following equation explicitly:

$$\int_\Omega W_u \Delta U_i \,\mathrm{d}\Omega = \int_\Omega W_u \Delta \tilde{U}_i \,\mathrm{d}\Omega - \Delta t \int_\Omega W_u \left(\frac{\partial p^n}{\partial x_i} + \theta_2 \frac{\partial \Delta p}{\partial x_i}\right) \mathrm{d}\Omega - \frac{\Delta t^2}{2} \int_\Omega \frac{\partial}{\partial x_j}(u_j W_u) \frac{\partial p^n}{\partial x_i} \,\mathrm{d}\Omega \tag{12}$$

where $\Delta U_i = U_i^{n+1} - U_i^n$. In the equation above, test function is momentum shape function W_u and θ_2 is taken as 1 for the explicit formulation.

4.4. Energy equation

Weak form of the energy equation with shape function of the energy (W_E) as the test function is given in the following form:

$$\int_\Omega W_E \Delta(\rho e)\,\mathrm{d}\Omega = \Delta t \left[-\int_\Omega W_E \frac{\partial}{\partial x_i}(u_i(\rho e + p))\,\mathrm{d}\Omega - \int_\Omega \frac{\partial W_E}{\partial x_i}\left(\tau_{ij}u_j + k\frac{\partial T}{\partial x_i}\right)\mathrm{d}\Omega\right]^n + \frac{\Delta t^2}{2}\left[\int_\Omega \frac{\partial}{\partial x_j}(u_j W_E)\left[\frac{\partial}{\partial x_i}(-u_i(\rho e + p))\right]\mathrm{d}\Omega\right]^n + \Delta t\left[\int_\Gamma W_E\left(\tau_{ij}u_j + k\frac{\partial T}{\partial x_i}\right) n_i \,\mathrm{d}\Gamma\right]^n \tag{13}$$

where total energy per unit volume is denoted by $E = (\rho e)$ and $\Delta E = E^{n+1} - E^n$.

4.5. Solution strategy

Solution procedure for the semi-implicit form of the CBS algorithm with temperature-jump and slip-velocity condition can be summarized as follows:

1. Solve the energy equation (13) with temperature-jump value on the wall and obtain E^{n+1};
2. Solve the fractional momentum equation (9) without any boundary condition;

3. Guess a temperature T_g from E^{n+1} using previous time step value of density and velocity field;
4. Solve the continuity equations (10) using T_g value and obtain p^{n+1}. Apply slip-velocity condition on the wall;
5. Solve the final step of the momentum equation (12) and obtain new momentum values;
6. Obtain ρ^{n+1} from the equation of state (3) using new pressure values. Then obtain velocity field from the momentum values;
7. Correct T_g using T^{n+1} obtained from E^{n+1} value by using new velocity u^{n+1} and density values ρ^{n+1};
8. Obtain temperature-jump and slip-velocity value at the wall substituting new velocity and temperature values within (7) and (8);
9. Check convergence; If not satisfactory, go to step 4;

It is reported in Reference [10], that there is no difference either in the numerical results or in the convergence behaviour of the CBS algorithm if more than two iterations are done. Since steady state solution is of interest, maximum iteration number is taken as 2 within the computation in this study except the early time steps in where the maximum iteration number is 3.

In the present study, pseudo-quadratic velocity/linear pressure interpolation elements (pP2P1) are used in computations [13]. The solution obtained using this kind of elements can be considered to be obtained on two different grids for the velocity and pressure solutions. Using pP2P1 type elements instead of P1P1 type elements makes the stiffness matrix in the continuity equation four times smaller for 2-D problems. Since the continuity equation forms the implicit part of the CBS algorithm, any reduction in the size of this equation reduce the storage requirements and number of calculations. It is reported that computational times are reduced up to 59% when pP2P1 type FEM elements are used within the CBS algorithm instead of P1P1 type elements while this ratio is 56% for alternative Petrov–Galerkin FEM method [13].

For the pressure driven compressible internal flows, locally very high pressure gradients and high velocities may be observed at the initial steps of the analysis if the initial solution is not a very good approximation of the steady state solution. When microfluidic boundary conditions are used, these initial disturbances produce unrealistic slip and temperature-jump values and cause the inner iterations of the CBS algorithm to diverge. Therefore, it is important to use no-slip conditions for the initial steps of the analysis.

5. RESULTS AND DISCUSSION

5.1. Straight micro channel

To verify the second-order slip-velocity boundary condition within the CBS algorithm, straight micro channel is selected as a test case. Pressure ratio of the channel inlet to the outlet (Π) is equal to 2.28 and outlet Knudsen number (Kn_{out}) is equal to 0.2 . The flow is assumed to be isothermal and reference temperature is taken as 273 K. Fifty-three and 21 grid points are taken in horizontal and vertical direction for the velocity mesh (see Figure 1). Total number of triangular elements used for the velocity calculation is 2080. The ratio of the channel length to the height (L/h) is equal to 20 and working fluid is Nitrogen with specific heat ratio of 1.4.

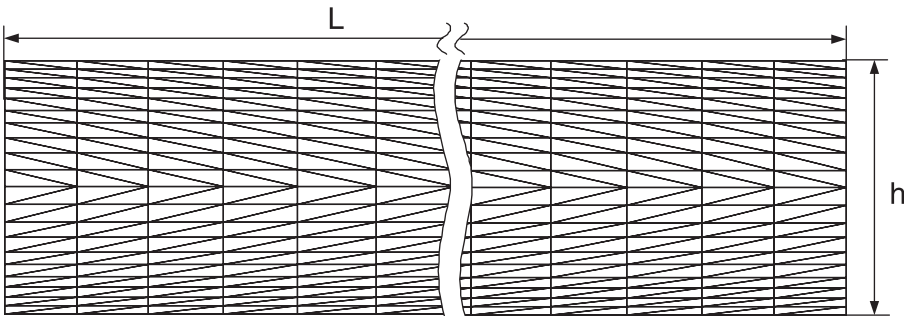

Figure 1. Velocity mesh of straight micro channel.

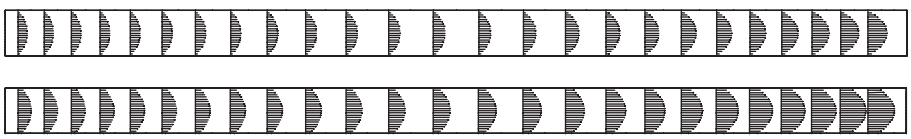

Figure 2. Velocity distribution along the straight micro channel with no-slip (upper) and slip-velocity (lower) boundary conditions.

The velocity vectors obtained using no-slip (NS) and with slip-velocity (WS) boundary conditions are plotted for comparison in Figure 2. The increase in the slip-velocity along the channel walls can be seen in the figure.

The pressure values are prescribed at the channel inlet and the outlet according to the selected value of the *Kn* and pressure ratio. Pressure distribution along the channel centreline is plotted in Figure 3. Both results with slip and no-slip boundary conditions are in good agreement with the other results presented in References [16, 17]. Nonlinearity in pressure distribution shows the compressibility effect along the channel.

Beskok has studied the same geometry with diatomic nitrogen as working fluid, using DSMC and μFlow (spectral-element-based continuum CFD solver) [16]. N–S and Burnett equations solver are used by Agarval and Yun [17] for the same geometry also. Baysal and Aslan [5] used N–S solver with first- and second-order slip-velocity boundary condition for the solution of the same problem. Obtained slip-velocity distribution along the channel wall, normalized with the inlet centreline velocity, are presented and compared with references in Figure 4. The result obtained using CBS algorithm with second-order slip-velocity boundary condition is in good agreement with the References [5, 17]. Maximum difference in magnitude between the computed slip-velocity and Reference [5] is less than 1%.

In order to assess the grid dependency of the results, analyses on several grids with different number of elements and element size distributions are performed. The grids used for this purpose are listed in Table I. First three grids contain the same number of elements but different grid stretching factors normal to the boundary. The resulting element sizes at the boundary of these grids are also listed in the table. The last grid on the other hand, has more elements. The slip velocity at the boundary is compared for these grids in Table I. It is

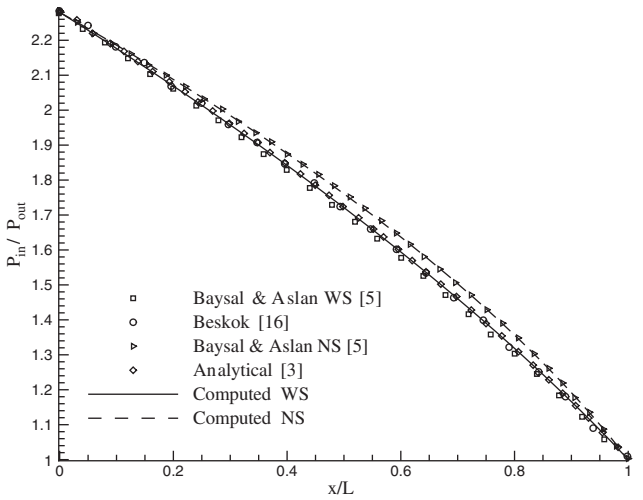

Figure 3. Pressure distribution along the straight micro channel centreline, $Kn_{\text{out}} = 0.2$.

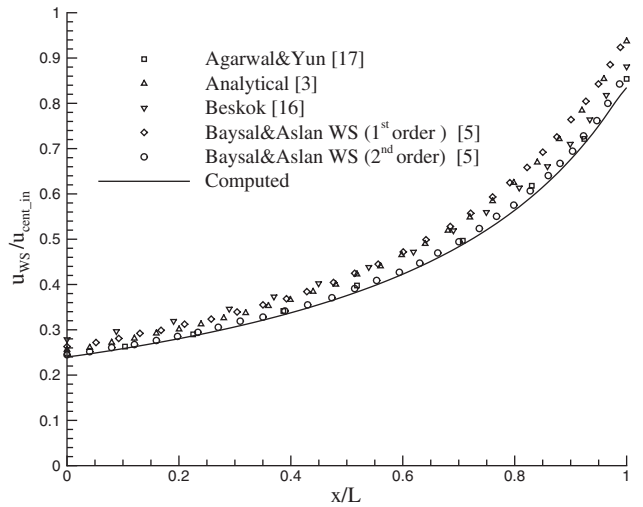

Figure 4. Slip velocity variation along straight micro channel wall, $Kn_{\text{out}} = 0.2$, $\Pi = 2.28$.

shown that the maximum difference in magnitude between the slip-velocity values obtained using different meshes is less than 2%.

The obtained velocity distributions and comparisons show that, the implementation of second-order slip-velocity boundary condition to the CBS algorithm yields accurate results for this test case.

Table I. Slip-velocity variation for different grids used in computation of micro channel flow.

Grid size	Normal distance of the first node	Maximum slip velocity difference
51×13	0.0196	0.7%
51×13	0.0173	0.9%
51×13	0.0136	1.3%
53×21	0.0336	Reference

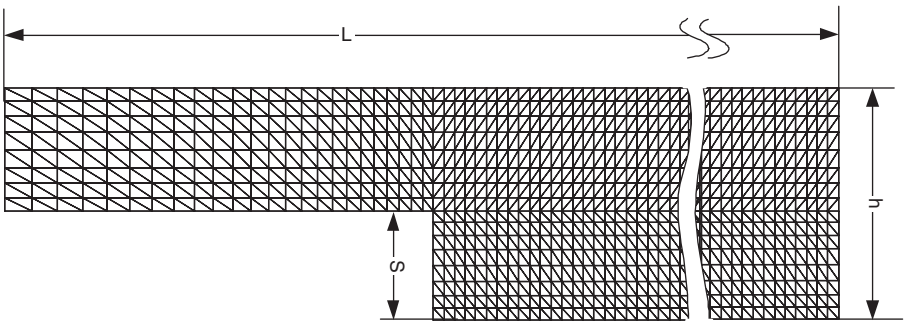

Figure 5. Pressure mesh of micro step duct.

5.2. *Separated flow in micro backward facing step*

To investigate the effect of second-order slip-velocity and temperature-jump boundary conditions on an internal micro-flow with separation, backward facing step geometry is selected as another test case. There are sharp gradients in flow field, which affect the mean free path and wall shear stress. The ratio of the channel length (L) to the exit height (h) is 5.6. The channel entry is also included to the simulation and it is located at $x/h = 0.86$. Ratio of step height (S) to the height of the channel h is 0.467. pP2P1 type of elements are used for these computations. The computational grid consists of 11 776 velocity elements and 2944 pressure elements. The grid, used for pressure calculations, is shown in Figure 5.

As a verification study for this type of flow problem, first, a case with inlet to outlet pressure ratio $\Pi = 2.32$, nitrogen as the working fluid and Kn at the outlet equal to 0.018 is analysed and the results are compared with Baysal and Aslan [5] and Beskok [16].

As in the straight micro channel, pressure is prescribed at the inlet and the outlet of the micro step duct geometry. On the solid wall, second-order slip-velocity and temperature-jump boundary conditions are employed (the wall surfaces are kept at 300 K). At the inlet, temperature value is prescribed as 330 K and vertical component of the velocity is set as zero. At the outlet, boundary term (traction) on the right-hand side of Equation (9) is taken into account.

Velocity profiles, local Kn and temperature distribution are given in Figure 6. As seen in the figure, fluid accelerates near the step expansion. So, high temperature gradient occurs at

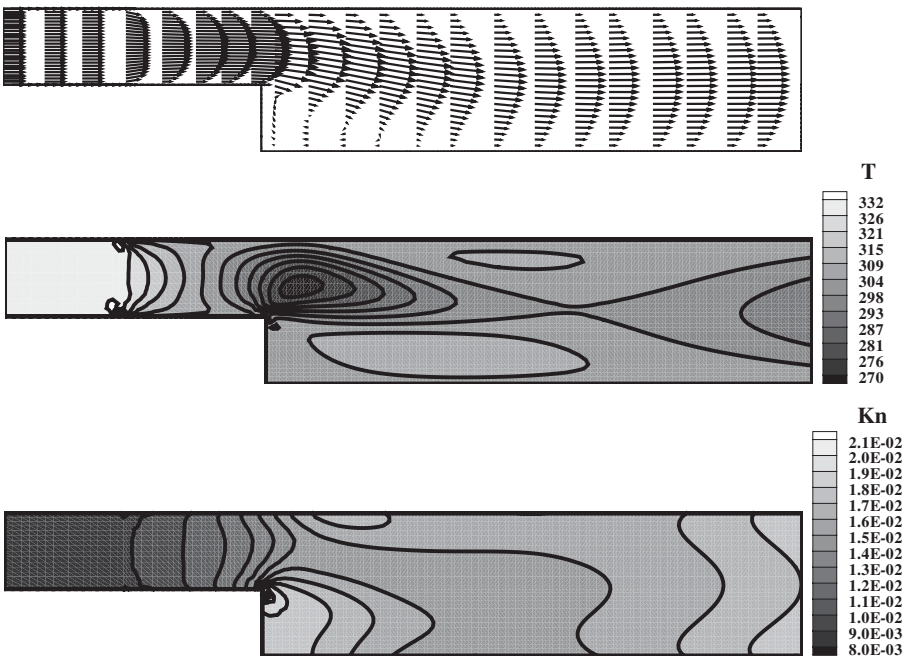

Figure 6. Velocity vectors, temperature and local *Kn* variation through the micro step duct, $Kn_{\text{out}} = 0.018$, $\Pi = 2.32$.

this region. Change in local *Kn* value due to adverse pressure gradient near the recirculation region can be also seen in the figure. Variation of the normalized streamwise velocity at five normal locations are plotted and compared with the results of Reference [5] in Figure 7. Pressure is normalized using dynamic head at the inlet and compared with the results of References [5, 16] in Figure 8. *Kn* distribution along the centreline of the micro step duct is given in Figure 9. As shown in these figures, results presented for this test case are in good agreement with reference studies.

In order to observe the effect of slip-velocity and temperature-jump on micro flows with separation, flow in a step duct is analysed for various channel sizes but the same inlet and outlet pressures. Selected channel heights results in a *Kn* range covering most of the slip-flow regime. For all cases, analyses are performed for both no-slip and slip-velocity boundary conditions. The variation of mass flow rate difference between the results obtained using no-slip and slip-velocity boundary conditions, with Knudsen number is presented in Figure 10. The results show that, as the Knudsen number increases, mass flow rate difference between the results obtained using no-slip ($\dot{m}_{\text{NS}}$) and slip-velocity ($\dot{m}_{\text{WS}}$) boundary condition increases. The change in inflow Mach number (Ma_{in}) with duct size is plotted in Figure 11 for both no-slip and slip model assumptions. As expected, Ma_{in} decreases with increasing *Kn* value. It is always higher for slip model compared to the no-slip case. These show that there is considerable difference between the results obtained using continuum models with no-slip boundary condition and the results obtained with slip-velocity, implemented to represent rarefaction effect.

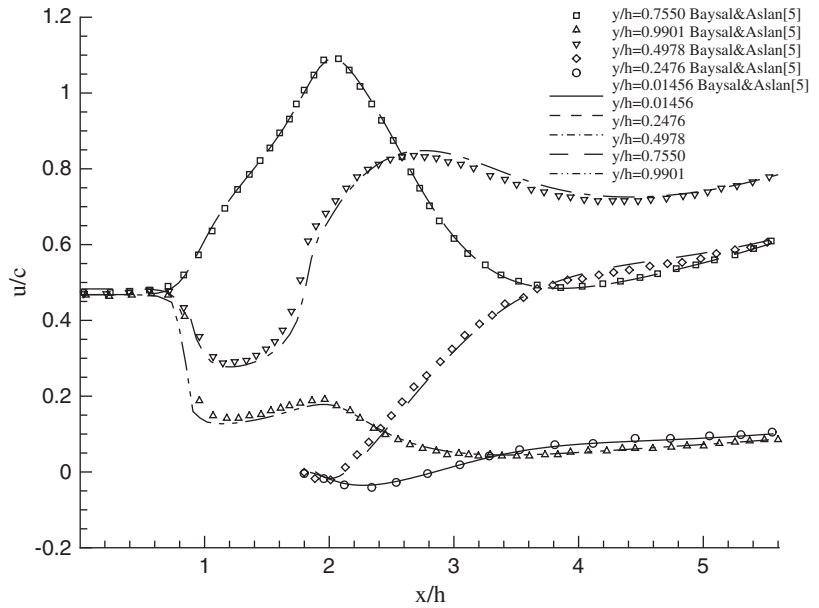

Figure 7. Comparison of normalized streamwise velocity with Baysal and Aslan [5], $Kn_{\text{out}} = 0.018$, $\Pi = 2.32$.

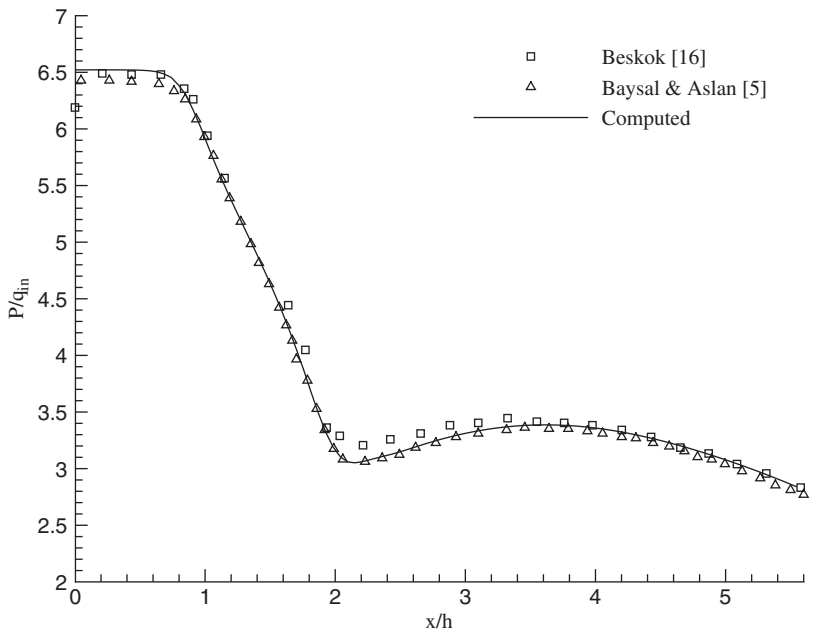

Figure 8. Pressure variation along the channel, $Kn_{\text{out}} = 0.018$, $\Pi = 2.32$.

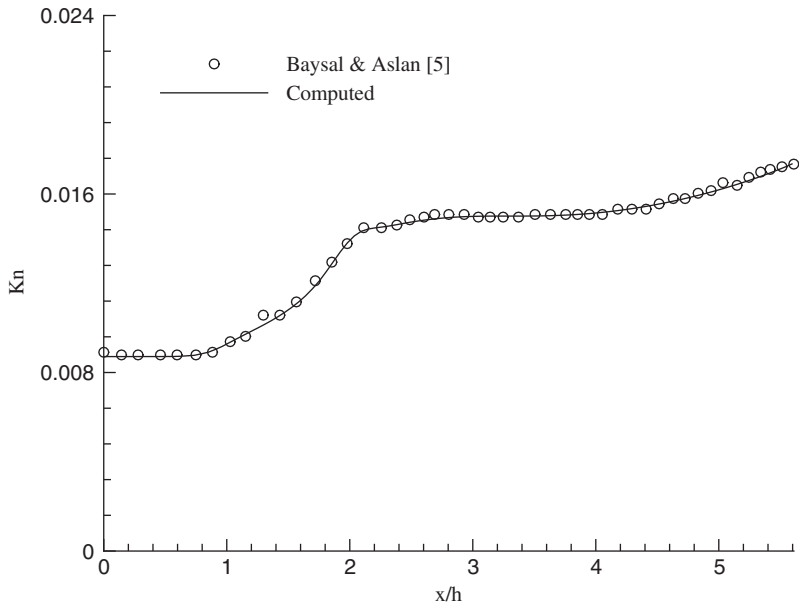

Figure 9. Local Kn along the centreline of the step duct geometry, $Kn_{\text{out}} = 0.018$, $\Pi = 2.32$.

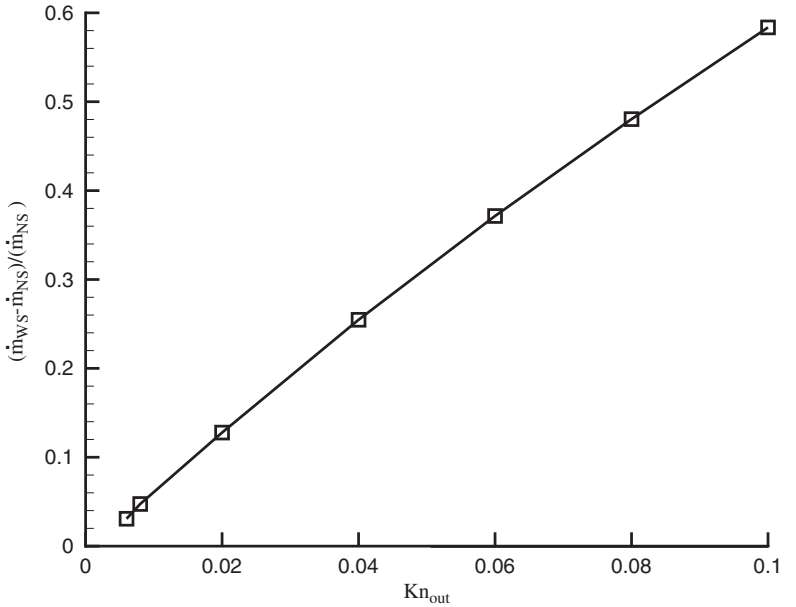

Figure 10. Variation of mass flow rate difference between the results obtained using no-slip and slip-velocity boundary conditions, with Knudsen number.

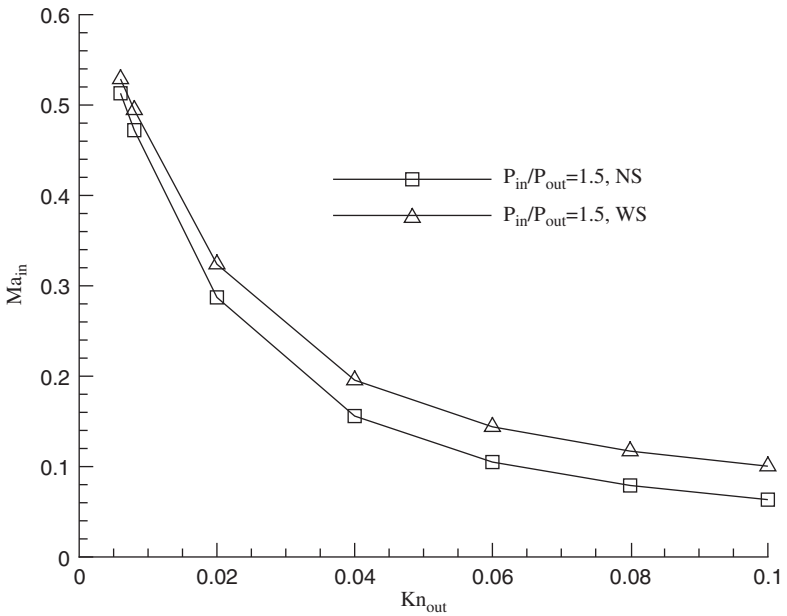

Figure 11. Variation of inlet Mach number with Knudsen number for the same inlet/outlet pressures.

Another set of analyses is run to observe the dependence of driving pressure difference to the Knudsen number for two different inlet Mach numbers, 0.287 and 0.405. In Figure 12, the variation of inlet to outlet pressure ratios with Knudsen number is plotted for two different inlet Mach numbers. Results obtained with no-slip and slip conditions are plotted together for comparison. As expected, increased inlet Mach number requires increased driving pressure difference. Similarly, the difference between slip and no-slip solutions increases with increasing Mach number as well as increasing Knudsen number. The variation of the mass flow rate difference between the slip and no-slip cases with Knudsen number is plotted in Figure 13. It is shown that the difference is limited for high inlet Mach number. The slip model employed (8) relates slip velocities to local Knudsen number, velocity and temperature gradients at the wall. Increased slip velocity on the other hand, results in reduced velocity gradient at the wall. This balance may explain the asymptotic behaviour of mass flow rate difference with increasing *Kn*. Additionally, increased temperature gradients at high inlet Mach numbers, increase second-order contribution of the thermal creep term in (8), yielding a higher slope for the flow rate difference vs *Kn* curve at low *Kn*. Another important feature of the flow is the reattachment length. In this study, the reattachment length, X, is used in normalized form with the channel height. In Figure 14, variation of the relative difference of the reattachment length between slip and no-slip cases are plotted against Knudsen number. Its behaviour is similar to the behaviour of the mass flow rate. For low Mach numbers, the difference increases almost monotonously. For high Mach numbers however, the difference presents an asymptotic behaviour. The variation in asymptotic behaviours seen in the mass flow rate and reattachment graphics is a result of extra slip generated by thermal creep for the high Mach number flow where temperature gradients are relatively higher.

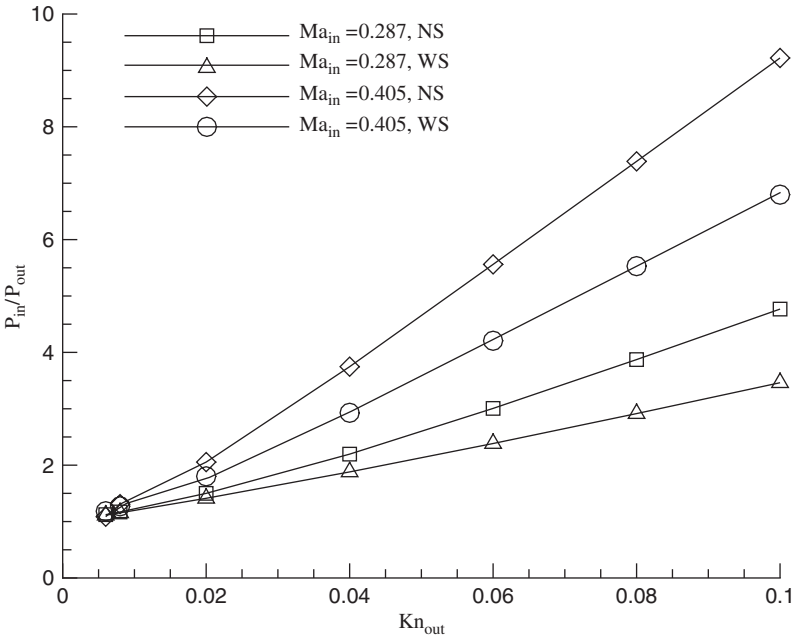

Figure 12. Inlet to outlet pressure ratios vs Knudsen number.

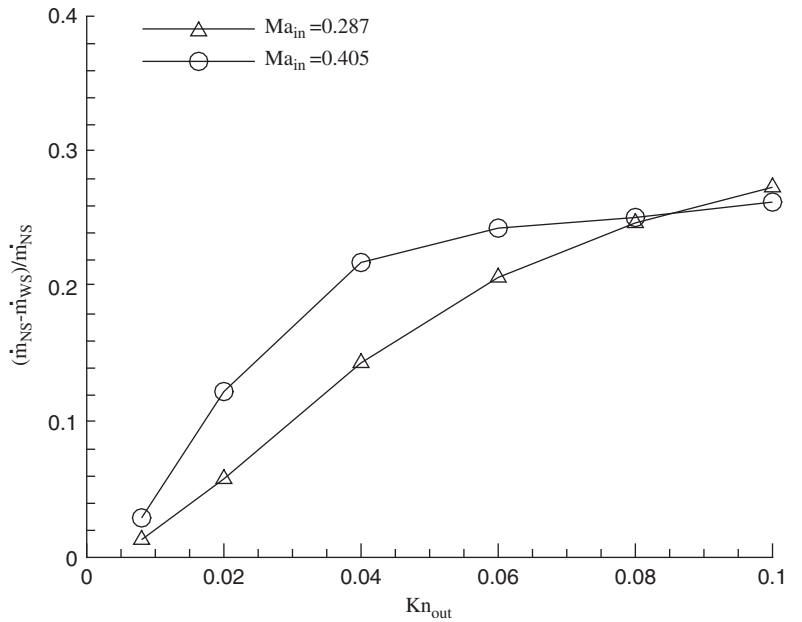

Figure 13. Mass flow rate difference between the results with no-slip and slip-velocity boundary conditions.

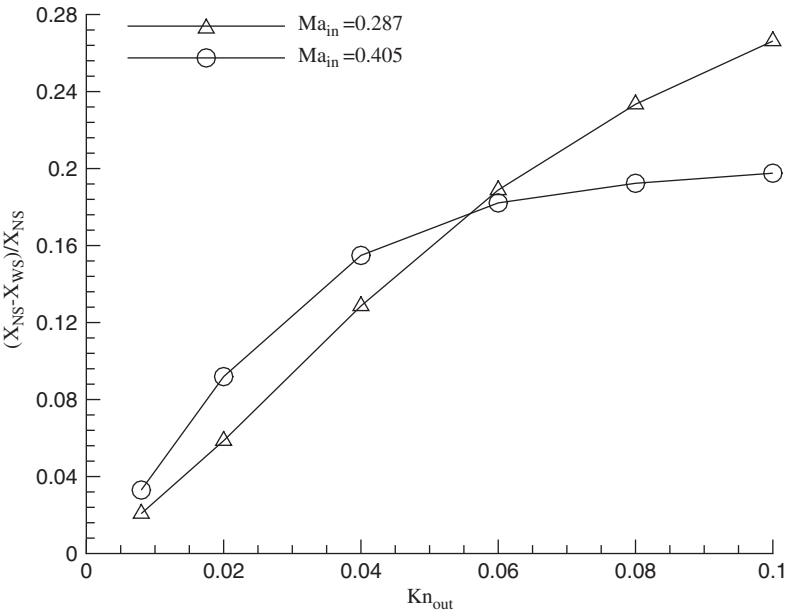

Figure 14. Reattachment length difference between the results with no-slip and slip-velocity boundary conditions.

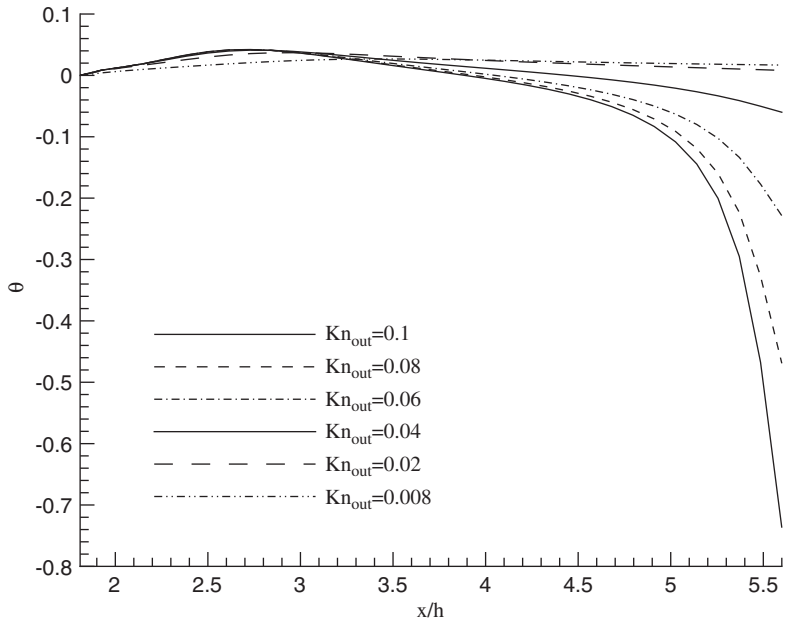

Figure 15. Temperature-jump along the lower wall for cases $Ma_{\text{in}} = 0.405$.

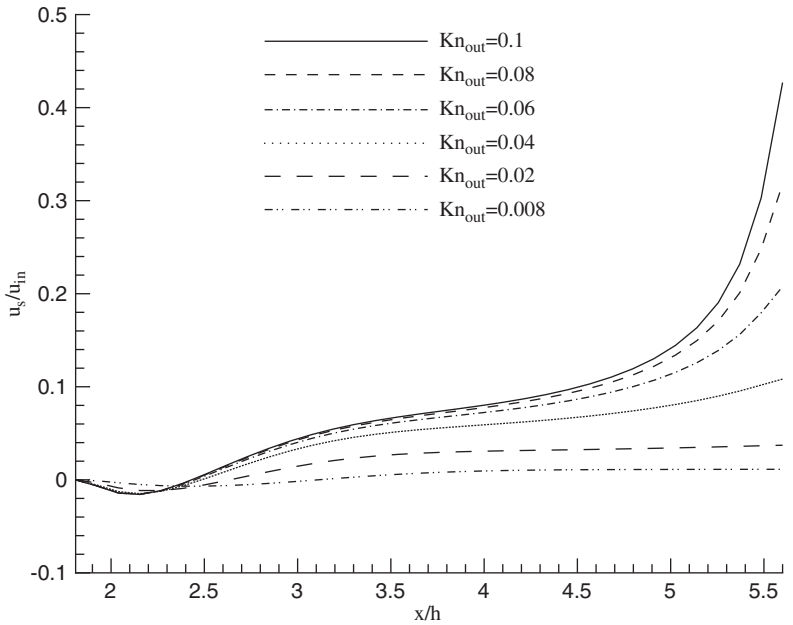

Figure 16. Slip-velocity along the lower wall for cases with $Ma_{in} = 0.405$.

The variation of non-dimensional temperature-jump, $\theta = (T - T_{wall})/(T_{inlet} - T_{wall})$, along the lower wall is presented in Figure 15. In this expression, T denotes the temperature of the fluid at the wall. As seen in the figure, for the higher Knudsen number flows temperature-jump values are very high compared to low Knudsen number ones. Furthermore, increased temperature gradients due to the accelerated flow towards the exit results in an increased temperature-jump compared to upstream stations. Similarly, the variation of the slip velocity, u_s, normalized with the inlet velocity, u_{in}, along the lower wall is plotted in Figure 16 for different Knudsen numbers and selected inlet Mach number of 0.405. The extra slip due to the high temperature jump is also observed for greater value of Kn towards the channel exit.

6. CONCLUSIONS

In this study, slip-velocity and temperature-jump boundary conditions are implemented within the CBS algorithm to solve compressible flows through micro-fluidic devices. Steady state solution is obtained using semi-implicit version of the algorithm with pP2P1 type of elements. The undesirable cost of using the semi-implicit version of the algorithm is reduced by using these types of elements. Comparison of the results obtained for pressure driven flows in straight and suddenly expanding micro channels with available numerical data and analytical models, shows that this implementation of the CBS algorithm is applicable and effective for these problems. Further analysis of micro step duct presents increasing effect of temperature-jump and slip for increasing Knudsen numbers. This effect, however, is limited, especially for high Mach number flows.

ACKNOWLEDGEMENTS

The support of Istanbul Technical University, under project number 1839 is acknowledged.

REFERENCES

1. Gad-el-Hak M (ed.). *MEMS Handbook*. CRC Press: New York, 2002.
2. Gad-el-Hak M. Flow physics in MEMS. *Mecanique and Industries* 2001; **2**:313–341.
3. Beskok A, Trimmer W, Karniadakis GE. Rarefaction and compressibility effects in gas microflows. *Journal of Fluids Engineering* 1996; **118**(2):448–456.
4. Beskok A, Karniadakis GE. A model for flows in channels, pipes and ducts at micro and nano scales. *Microscale Thermophysical Engineering* 1999; **3**:43–77.
5. Baysal O, Aslan AR. Computing separated flows in MEMS devices. In *Proceedings of ASME Fluids Engineering Division Summer Meeting*, Montreal, Quebec, Canada. *Paper No. FEDSM2002-31157*, July 14–18, 2002.
6. Chorin AJ. Numerical solution of Navier–Stokes equations. *Mathematics of Computation* 1968; **22**:745–762.
7. Zienkiewicz OC, Wu J. A general explicit or semi-explicit algorithm for compressible and incompressible flows. *International Journal for Numerical Methods in Engineering* 1992; **35**:457–479.
8. Zienkiewicz OC, Codina R. A general algorithm for compressible and incompressible flow, part I. The split characteristic based scheme. *International Journal for Numerical Methods in Fluids* 1995; **20**:869–885.
9. Zienkiewicz OC, Satya Sai BVK, Morgan K, Codina R, Vazquez M. A general algorithm for compressible and incompressible flow—part II. Tests on the explicit forms. *International Journal for Numerical Methods in Fluids* 1995; **20**:887–913.
10. Codina R, Vazquez M, Zienkiewicz OC. A general algorithm for compressible and incompressible flows, part III—a semi-implicit form. *International Journal for Numerical Methods in Fluids* 1998; **27**:12–32.
11. Zienkiewicz OC, Nithiarasu P, Codina R, Vazquez M, Ortiz P. An efficient and accurate algorithm for fluid mechanic problems. The characteristic based split (CBS) algorithm. *International Journal for Numerical Methods in Fluids* 1999; **31**(1):359–392.
12. Zienkiewicz OC, Satya Sai BVK, Morgan K, Codina R. Split characteristic based semi-implicit algorithm for laminar/turbulent incompressible flows. *International Journal for Numerical Methods in Fluids* 1998; **23**: 787–809.
13. Edis FO, Aslan RA, Celik B. Implementation of pseudo-second order velocity interpolation within the characteristic-based-split procedure. In *Proceedings of ECCOMAS 2001*, *on CD-Rom European Congress on Computational Methods in Applied Sciences and Engineering*, Swansea, Wales, U.K., 2001. ISBN 0 905 091 12 4.
14. Nithiarasu P, Zienkiewicz OC, Satya Sai BVK, Morgan K, Codina R, Vazquez M. Shock capturing viscosities for the general fluid mechanics algorithm. *International Journal for Numerical Methods in Engineering* 1998; **28**:1325–1353.
15. Nithiarasu P. On boundary conditions of the characteristic based split (CBS) algorithm for fluid dynamics. *International Journal for Numerical Methods in Engineering* 2002; **54**:523–536.
16. Beskok A. Molecular based microfluidic simulation models. In *MEMS Handbook*, Gad-el-Hak M (ed.). CRC Press: New York, 2001; 8.1–8.28.
17. Agarwal R, Yun K. Burnett simulations of flow in microdevices. In *MEMS Handbook*, Gad-el-Hak M (ed.). CRC Press: New York, 2001; 7.1–7.36.

